ACS APPLIED MATERIALS & INTERFACES

www.acsami.org

Research Article

Photosensitive Composite Inks for Digital Light Processing Four-Dimensional Printing of Shape Memory Capture Devices

Linlin Wang, Fenghua Zhang, Yanju Liu, Shanyi Du, and Jinsong Leng*

Cite This: *ACS Appl. Mater. Interfaces* 2021, 13, 18110–18119

Read Online

ACCESS | Metrics & More | Article Recommendations | Supporting Information

ABSTRACT: High-performance shape memory thermosetting polymers and their composites for four-dimensional (4D) printing are essential in practical applications. To date, most printable thermosets suffer from complicated processes, poor thermodynamic performances, and low printing speed. Here, photosensitive composite inks for fast photocuring printing are developed. The inks consist of epoxy acrylate (EPAc), polyethylene glycol dimethacrylate (PEGDMA), and carbon fillers, which form a firm network structure when exposed to UV light. EPAc is synthesized via addition esterification of epoxy resin and acrylic acid under mild conditions. It is worth noting that raw materials for the reaction are diverse, including not only various epoxy resins but also molecules with epoxy groups. The 4D printing speed of up to 180 mm/h is mainly attributed to the exothermic reaction initiated by free radicals, which accelerates the polymerization of EPAc and PEGDMA. Most importantly, by increasing the exposure time of each layer from 1 s to 3 s during the printing process, the epoxy composite-infilled carbon nanotubes and carbon fibers are printed to ensure the integrity of the microlayer structure. Furthermore, we design a claw-like catcher device based on the above printable composite inks to demonstrate its potential applications in aerospace, such as grasping end-of-service spacecraft or explosive debris. Undoubtedly, 4D printing technology opens up a new portal for the manufacturing of thermoset epoxy composites and complex structures, which make the shape memory thermosetting epoxy resins and their composites possess excellent properties and good engineering application prospects.

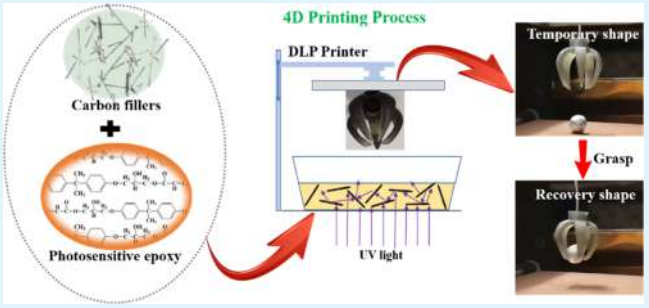

KEYWORDS: *shape memory polymers, composite inks, photosensitive epoxy resin, 4D printing, capture device*

1. INTRODUCTION

In the past few decades, the molding of materials has relied on traditional manufacturing processes, such as injection molding, casting, and extrusion.[1−3] There is no doubt that it is difficult to produce and incorporate highly complex parts or structures using these traditional manufacturing techniques. Therefore, it is of great necessity to develop new materials and new manufacturing technologies. Shape-memory polymer (SMP) is a kind of representative smart material and it can recover from a special temporary shape to its original shape under external stimuli.[4−9] Compared to shape-memory alloys, SMPs show low density, low activation temperature, low cost, high elastic deformation, and promising biocompatibility as well as biodegradability.[10] Besides, SMPs have great application potential in aerospace, biomedical field, bionics, tissue engineering, and robotics.[11−17]

Shape-memory epoxy is a typical thermosetting polymer, which is commonly used in resin matrix composites.[18−21] With the emergence of three-dimensional (3D) printing technology, printable epoxy resins (EPs) have attracted widespread attention. There are two main ways to print EPs. One is to add fillers into the resin, which plays a supporting role in the printing process to ensure that the printed structure will not collapse. Rodriguez et al.[22] added carbon nanofibers as fillers to the hybrid of epoxidized soybean oil and bisphenol F diglycidyl ether to prepare printable inks. The printed origami structures were heat-cured. Similarly, Fang et al.[23] used EPs and continuous carbon fibers (CFs) to print heat-cured grid structures. The structures printed in this way have low precision and poor stability. The other method is to mix the epoxy with the photosensitive resin, which is light-cured during the printing process and then heat-cured after printing. Some researchers used this two-stage curing method to improve the properties of 3D printable materials.[24−29] There are two kinds of network structures in photothermal curing resins, called interpenetrating networks. One is the photocuring network structure and the other is the thermocuring network structure. The disadvantage of this method is that the internal stress of the printed structure is released during the thermal curing

Received: February 7, 2021
Accepted: April 1, 2021
Published: April 12, 2021

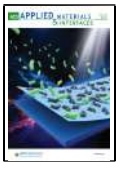

https://doi.org/10.1021/acsami.1c02624
ACS Appl. Mater. Interfaces 2021, 13, 18110−18119

process, which leads to structural deformation. Another disadvantage is that the heat resistance of the photocuring network structure is low, which might be more easily destroyed compared with the thermo-curing network structure. To make the epoxy-forming process faster and easier, one-step molding of printable epoxy was developed.

The strength of pure EPs is not sufficient enough to meet the requirements of space applications, so it is necessary to investigate epoxy composites. Fillers are often used to improve the thermodynamic properties of resins, such as graphene, CFs, glass fibers, SiO_2 particles, steel fibers, and magnetic particles. Graphene as a filler improves not only the mechanical property of 3D printed resin but also thermal conductivity and electrical conductivity.[27,28,30,31] In addition, it has been reported that SiO_2 particles can promote the photocuring of resins. Choong et al.[32] found that the curing time of photosensitive resins infilled with 20 nm SiO_2 nanoparticles was significantly shortened. Kuang et al.[33] incorporated SiO_2 particles in the resin to enhance the shear-thinning effect and maintain the printed structure. The filler is randomly distributed in the ink, and the isotropic material is prepared. Fillers in the ink can also have an oriented arrangement, so that the material is anisotropic. Ren et al.[34,35] selected short steel fibers as reinforcing materials to enhance the photosensitive resins. The oriented arrangement of the steel fibers in the magnetic field can not only enhance the matrix material but also control the deformation of the material. Carbonyl iron powders were dispersed in the matrix, generating chain clusters of magnetic particles to drive artificial cilia in the magnetic field.[36] Kim et al.[37] studied the effect of two different nozzle shapes on the aligned/random distribution of silver nanowires, resulting in the change of dielectric constant of 3D printed samples. 4D printing has attracted extensive attention in various fields since the concept of 4D printing was put forward. Efficient 4D printing of high-performance epoxy composites has been put on the agenda.

In this work, we synthesized photosensitive epoxy acrylate (EPAc) via addition esterification reaction between bisphenol A EP and acrylic acid (AA). Network structures were formed by polymerization of EPAc and polyethylene glycol dimethacrylate (PEGDMA) when the inks were exposed to UV light. We investigated how the reactive diluent affects the cross-linking degree of the network and thermodynamic properties of the resin. Furthermore, the addition of carbon nanotubes (CNTs) or CFs made a difference to the cross-linking degree, microlayer structure, and heat conduction of the resin. The printed parts exhibited excellent shape memory effect, whose shape recovery rate (R_r) and shape fixity rate (R_f) were also revealed. This work was beneficial to broaden the variety of thermosets for 4D printing and it also provided a significant guidance for the performance optimization of other SMPs.

2. EXPERIMENTAL SECTION

2.1. Materials and Methods. *2.1.1. Materials.* Bisphenol A EP (E51) was produced by Nantong Xingchen Synthetic Materials Co. Ltd., China. AA, Toluhydroguinone (THQ), Triethylamine (TEA), PEGDMA (M_n = 550 g/mol), and 2,4,6-Trimethylbenzoyldiphenyl Phosphine Oxide (TPO) were purchased from Aladdin.

2.1.2. Synthesis of EPAc Ink. 0.4 mol (28.8 g) AA was poured into 0.2 mol (78.4 g) EP to obtain a mixed solution in a round-bottom flask with three necks, followed by the incorporation of 2.0 mmol (0.248 g) THQ and 4.0 mmol (0.56 ml) TEA. The mixture was heated to 75 °C and stirred at a constant speed for 6 h. 2.0 wt % TPO was added in the solution with unceasing stirring for 1 h to obtain the EPAc ink. In the reaction, THQ acted as the polymerization inhibitor and TEA acted as the catalyst. TPO was used as a photoinitiator.

2.1.3. Synthesis of Black EPAc + PEGDMA + CNT Inks. 0.07 mol (38.5 g) PEGDMA was poured into the above EPAc ink and stirred for 1 h to prepare the EPAc + PEGDMA ink. The role of PEGDMA was both as a soft segment and diluent. By adding different masses of multiwalled CNTs into the EPAc + PEGDMA ink, the inks with 0.5, 1.0, and 2.0 wt % CNTs were labeled EPAc + PEGDMA + 0.5CNT, EPAc + PEGDMA + 1.0CNT, and EPAc + PEGDMA + 2.0CNT, respectively.

2.1.4. Synthesis of the Black EPAc + PEGDMA + CF Ink. 0.07 mol (38.5 g) PEGDMA was poured into the above EPAc ink and stirred for 1 h to prepare EPAc + PEGDMA ink. The role of PEGDMA was both as a soft segment and diluent. By adding CFs into EPAc + PEGDMA ink, the ink with 0.5 wt % CFs was labeled EPAc + PEGDMA + 0.5CF.

2.2. DLP Printing. The printer is Phoenix Touch Pro (Full Spectrum Laser, USA) with a UV LED. For the EPAc + PEGDMA ink, the adherence exposure time is 2 s, the slice exposure time is 1 s, and the top pause time is 2 s. For the EPAc + PEGDMA + 0.5CNT ink and EPAc + PEGDMA + 0.5CF ink, the adherence exposure time is 6 s, the slice exposure time is 3 s, and the top pause time is 6 s. The light intensity was 59.4 mW/cm^2, measured using a THORLABS PM100D irradiance meter.

2.3. Characterization and Measurements. The ink viscosity was measured using a Discovery Hybrid rheometer (TA Instruments, USA) at 25 °C with a gap of 1000 μm. EP and EPAc were dissolved in deuterated chloroform ($CDCl_3$) for nuclear magnetic resonance (NMR, Bruker AVANCE III 400M, Switzerland). The addition esterification reaction was monitored using a ReactIR 702L detector (Mettler-Toledo, Switzerland) with a range of 3000−800 cm^{-1} and 4 cm^{-1} resolution. The EP was characterized by attenuated total reflection Fourier transform infrared (ATRFTIR, Perkin Elmer Corporation, USA) with a range of 4000−400 and 4 cm^{-1} resolution. The viscoelasticity and glass transition temperatures (T_g) of UV curable samples were studied by dynamic mechanical analysis (DMA, TA Instruments DMA Q800, USA). Samples were printed as rectangular bars with a size of 30 × 5.0 × 1.0 mm. The test was carried out on DMA tensile clamping fixture with a dynamic frequency of 1 Hz, an amplitude of 20 μm, and a heating rate of 3 °C/min. The mechanical properties of tensile standard samples (ASTM D638, Type IV) were measured using an Instron 5500R universal testing machine (Instron Corp., USA) with an elongation of 1.0 mm/min. Thermogravimetric analysis (TGA) was performed using a thermogravimetric analyzer (Mettler-Toledo, Switzerland). The particulate samples were tested at a rate of 10 °C/min in nitrogen at a temperature between 25 and 800 °C. Structures of the printed layers and the dispersion of CNTs and CFs in the inks were observed using an optical microscope (Keyence VHX-900, Japan). The morphology of CNTs and CFs was exposed using a scanning electron microscope (SEM) (JSM-7600F, JEOL Ltd.). The samples were sputtered with gold for 30 s before observation.

2.4. Shape-Memory Behaviors. The shape-memory behaviors were examined by a bending test using rectangular strip specimens as the permanent shape and "U" as the temporary shape. R_f and R_r were calculated based on the following formulas

$$R_f = \frac{180^\circ - \theta_s}{180^\circ}$$

$$R_r = \frac{\theta_r}{180^\circ - \theta_s}$$

In the formulas, θ_s is the sagging angle when the external force is removed and θ_r is the shape recovery angle during the shape recovery.

3. RESULTS AND DISCUSSION

The reaction for synthesizing the photosensitive epoxy ink takes place in the resin synthesizer at a constant temperature as shown in Figure 1a. Figure S1 exhibits the reaction equation

https://doi.org/10.1021/acsami.1c02624
ACS Appl. Mater. Interfaces 2021, 13, 18110−18119

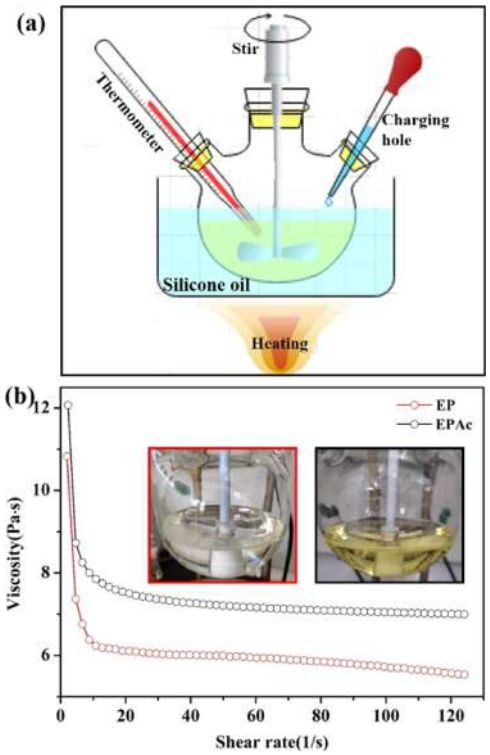

Figure 1. (a) Synthetic device of EPAc; (b) addition esterification; (c) viscosity versus shear rate curves of EP and EPAc; and (d) molecular weight distribution plot of EP and EPAc.

between EP and AA in the presence of a catalyst, which is essentially an addition esterification reaction between the epoxy and carboxyl groups.[38−40] Compared with the conventional esterification, no water is produced.[41] The ingredient EP is a colorless and transparent liquid and the reaction product EPAc is a yellow transparent liquid. The viscosity versus shear rate curves in Figure 1b show that the initial viscosity of EP and EPAc is 10.8 and 12.0 Pa·s, respectively. With the increase in shear rate, the viscosity decreases due to the molecular orientation. When the shear rate exceeds 20 1/s, the change is not obvious.

NMR is performed on the raw material EP and the reaction product EPAc to determine the reaction product and yield, and the results are shown in Figure S2. Hydrogen atoms in EP and EPAc are labeled from H_a to H_f. The peaks in 1H NMR of EP and EPAc were normalized. From the result, the integral height ratio of the peaks reveals the number ratio of protons, H_e or H_d:H_a or H_c:H_f = 4:2:6, which is corresponding to H atoms on benzene rings, $-CH_2-$ and $-CH_3$, respectively. After the reaction, the ambience of H_a atom changed, resulting in the decrease of peak (H_a) intensity and the formation of a new peak ($H_{a'}$) at the same time. The yield of the addition esterification reaction is calculated by the ratio of $H_{a'}$ to $H_{a'}$ + H_a, which is 68.2%.

The reactants and products in the reaction process can also be monitored in real-time using an infrared probe in the range of 3000 to 800 cm^{-1}. Figure 2a shows the 3D surface IR spectrum during the reaction. As the reaction proceeds, some peaks become higher and some become lower. Figure 2b shows the height variation of four characteristic peaks. The peak at 912 cm^{-1} (Figure 2c) is attributed to the epoxy group, whose height gradually declines, indicating the consumption of epoxy groups. The peaks at 1184 and 1728 cm^{-1} (Figure 2d,f) are attributed to the C−O bond and C═O bond in the ester group, respectively. The peak at 1412 cm^{-1} (Figure 2e) is assigned to −OH. The height of the three peaks increases slowly, which shows the formation of ester and hydroxy groups.

As the high viscosity of EPAc is not conducive to printing, PEGDMA is used as a diluent to reduce the resin viscosity which decreases from 12.0 to 6.6 Pa·s as shown in Figure 3a. Therefore, EPAc + PEGDMA resin is used as the ink of DLP printer, which is cured layer by layer under UV light. The TPO molecule absorbs UV radiation energy to produce free radicals, a trimethyl benzoyl radical and a diphenyl phosphoryl radical (Figure 3b), which initiate polymerization. A large amount of heat is released from the polymerization reaction, which facilitates the reaction to form chain polymerization. It is very difficult for the EPAc + PEGDMA ink to be completely polymerized in a short time only by the DLP printer, so it is necessary to post-cure the printed objects. The printed part is exposed to 365 nm UV light for 30 s. There are two reasons for the post-curing, one is to eliminate the influence of the photo-cross-linking gradient in the printing process and the other is to make the resin fully cross-linked. The illustrations in Figure 3d depict that EPAc and PEGDMA form a network structure through the polymerization. The blue wave line represents EPAc and the orange line represents PEGDMA. PEGDMA acts as not only a diluent but also as a modifier in the resin.

We printed some film samples to understand the curing of the resin during the printing process. The films with a thickness of 500 μm and different exposure times (1, 3, 5, and10 s) are printed and weighed. The cross-linking degree is tested by the equilibrium swelling method.[27,42,43] The printed films are soaked in acetone for 72 h to swell, dried at 80 °C for 2 h, and weighed again. The cross-linking degree values of the films are calculated and recorded, as shown in Figure 3e. For EPAc, the cross-linking degree increases with the increase in exposure time. When the exposure time is 1 s, the cross-linking degree is the minimum, which is 70.9%, whereas when the exposure time increases to 10 s, the cross-linking degree increases to 74.5%. For EPAc + PEGDMA, the cross-linking degree decreases slightly with the increase in exposure time from 86.4 to 85.9%. The results demonstrate that EPAc + PEGDMA is easier to polymerize than EPAc. The high viscosity of EPAc has a negative effect on the reaction rate due to poor molecular mobility. Therefore, the cross-linking degree of EPAc is lower than that of EPAc + PEGDMA. The uncross-linked vinyls in EPAc are more, which are marked with green circles in the network structure diagram.

Some information of the cross-linking degree can also be obtained from the infrared spectrum. Figure S3a shows the infrared spectrum of the printed film with an exposure time of 10 s. The broad peak at around 3446 cm^{-1} and the weak peak at 1407 cm^{-1} are attributed to the stretching vibration and bending vibration of −OH in EPAc, respectively. The absorption peaks at 2973, 2929, and 2863 cm^{-1} can be assigned to the symmetric stretching vibration of C−H in $-CH_3$ and $-CH_2-$.[44] The peak of the carbonyl group in the ester group shifts from 1720 to 1724 cm^{-1}.[45,46] It should be noted that the peaks at 1607, 1508, and 809 $cm^{-1}$are C−C bending vibration and C−H bending vibration in phenyl. Large quantities of vinyls are consumed during the curing process, and as a result, the C═C absorption peaks at 1635 cm^{-1} in EPAc and EPAc + PEGDMA are not obvious in the spectrum.[47] In addition, unreacted epoxy groups are detected

https://doi.org/10.1021/acsami.1c02624
ACS Appl. Mater. Interfaces 2021, 13, 18110−18119

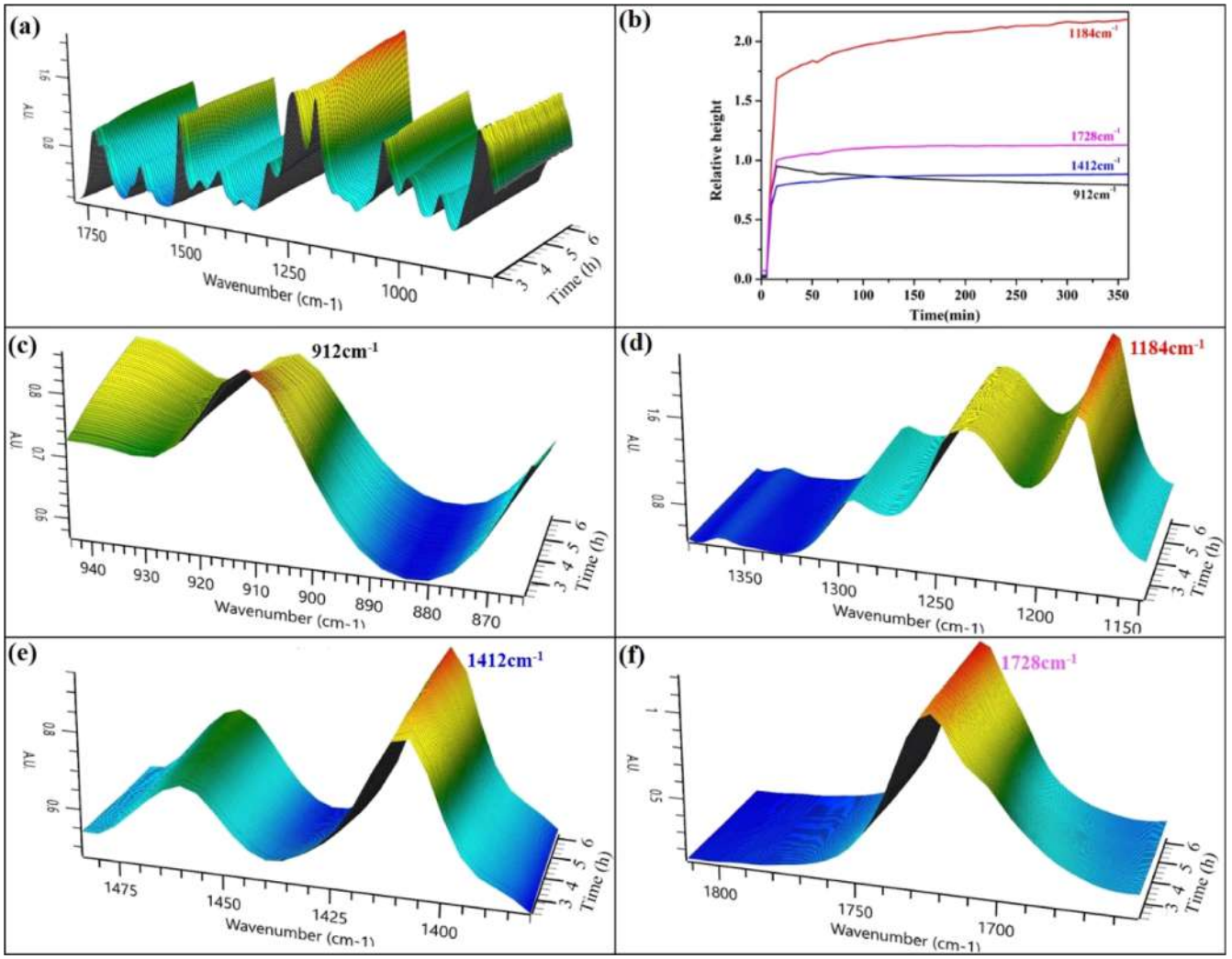

Figure 2. (a) 3D surface infrared spectrum during the reaction; (b) peak-height trend chart of four peaks; and (c–f) four peaks with a marked change in peak height.

at 912 cm^{-1}. Figure S3b,c shows the FTIR spectra of EPAc and EPAc + PEGDMA films with different exposure times (1, 3, 5, and 10 s). For EPAc, the peak intensity of 1 s exposure time is weaker than that of the other three peaks. The result shows that the cross-linking degree of EPAc is lower when the exposure time is 1 s, which is consistent with the result of the cross-linking degree. For EPAc + PEGDMA, the peak intensity does not change with different exposure times, indicating that there is no change in the degree of cross-linking, and the result is also consistent with the result of the cross-linking degree.

The higher the cross-linking degree is, the greater the storage modulus is. According to the results of the cross-linking degree, the storage modulus of EPAc + PEGDMA is higher than that of EPAc at room temperature. The DMA results of the two resins are shown in Figure S4a,b. The storage modulus (1.34 GPa) of EPAc + PEGDMA at 30 °C is indeed higher than that of EPAc (1.71 GPa), which is consistent with the results of the cross-linking degree. The temperature corresponding to the peak of the tan delta curve is defined as T_g. T_g of EPAc is 86.2 °C and T_g of EPAc + PEGDMA is 81.3 °C. The stress–strain curves of EPAc and EPAc + PEGDMA at room temperature are presented in Figure S4c. For EPAc, the stress–strain curve is approximately linear, indicating that brittle fracture occurs. There is no obvious yield phenomenon in the stress–strain curve of EPAc + PEGDMA. After that, the stress remains basically unchanged and the strain increases, indicating that EPAc + PEGDMA undergoes plastic deformation. The maximum strain of EPAc is 6.1% and that of EPAc + PEGDMA is 16.3%. The cross-linking degree not only affects the mechanical properties but also affects the heat resistance of the resin. The heat resistance of the resin is tested by TGA and the results are shown in Figure S4d. The initial thermal decomposition temperature of the two resins is 350.1 °C. There is no significant difference before 400 °C. After that, the weight of EPAc + PEGDMA decreases faster than that of EPAc due to the fracture of C–O bonds. The C–O bonds in $-C_6H_4-O-C_6H_4-$ are more stable than those in $-CH_2-O-CH_2-$. Therefore, more energy is needed to break the C–O bonds in EPAc. At 800 °C, the mass fraction of EPAc is 12.2% and that of EPAc + PEGDMA is 6.5%. The derivative thermogravimetry curve reflects the weight loss rate in the range of 290 to 550 °C, and the weight loss rate is the greatest at 419 °C.

To improve the strength, heat resistance, and thermal conductivity of the resin, adding some fillers, such as particles and fibers, can affect the curing process of the photosensitive resin. Figure 4a shows the SEM image of additive CNTs with an outer diameter of ~15 nm and a length of ~20 μm. The

https://doi.org/10.1021/acsami.1c02624
ACS Appl. Mater. Interfaces 2021, 13, 18110–18119

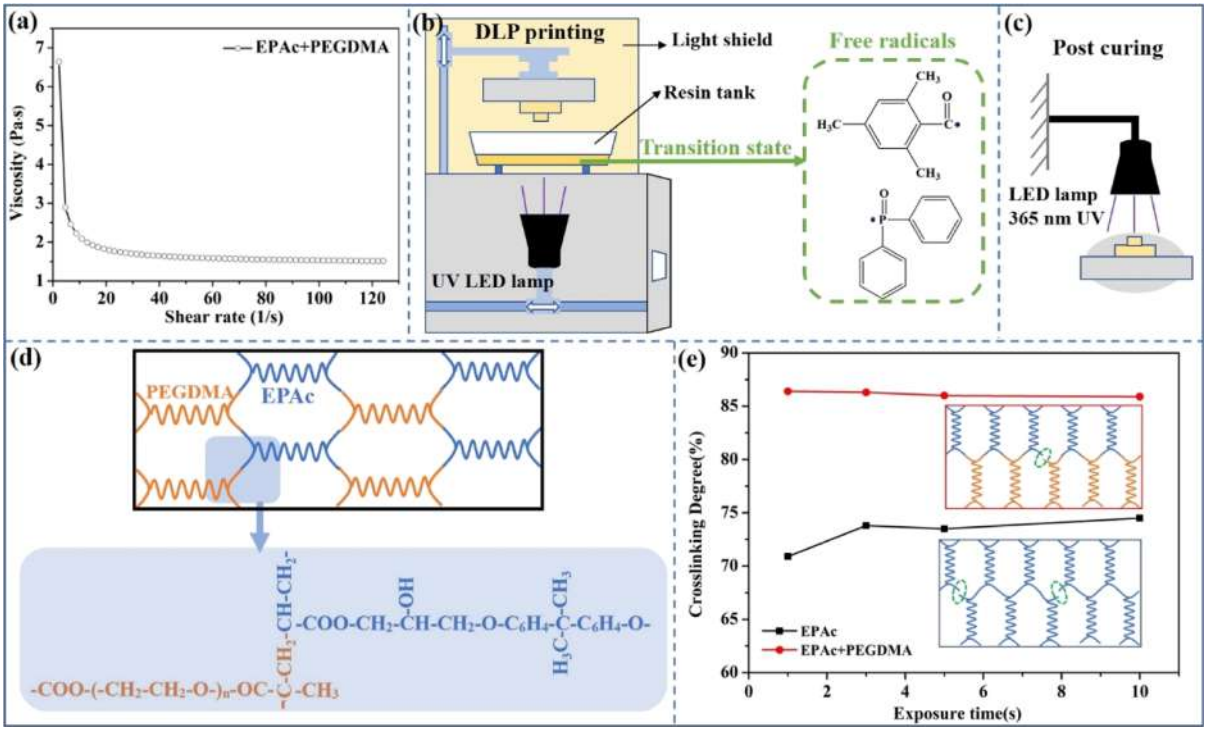

Figure 3. (a) Viscosity curve versus shear rate of EPAc + PEGDMA; (b) schematic diagram of the DLP printer and free radicals produced by the photolysis of TPO; (c) post-curing of the printed parts; (d) network structure formed by cross-linking and molecular structure of the network; and (e) cross-linking degree of EPAc and EPAc + PEGDMA resin.

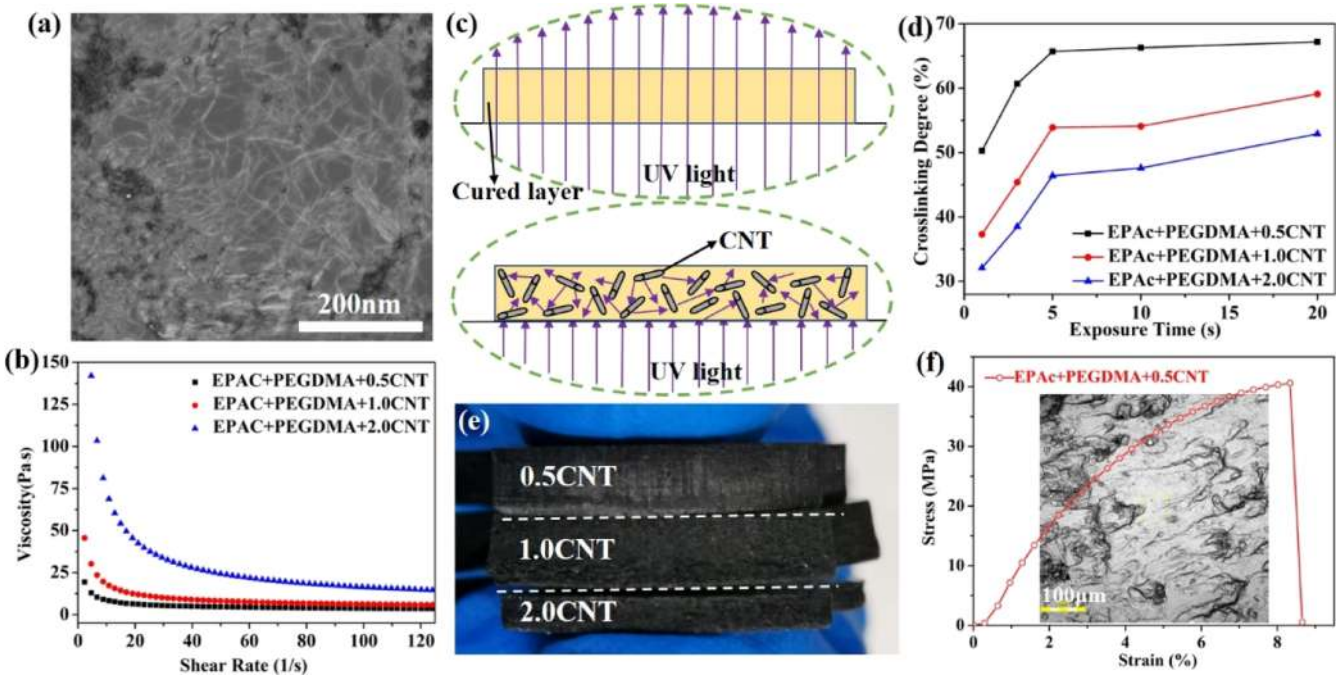

Figure 4. (a) SEM image of the additive CNTs; (b) effect of CNT concentration on the ink viscosity; (c) schematic diagram of the UV light path; (d) cross-linking degree of the cured resin; (e) side view of the pawl parts with different CNT concentrations; and (f) stress−strain behavior of EPAc + PEGDMA + 0.5CNT resin and the inset: a fracture surface optical micrograph.

addition of CNTs results in an increase in ink viscosity. The curves in Figure 4b show the viscosity change of the composite inks with the shear rate. The more the CNTs added, the greater the viscosity of the composite ink. The initial viscosity of the EPAc + PEGDMA + 0.5CNT ink is 19.3 Pa·s, which is about three times that of the EPAc + PEGDMA ink. In addition, the EPAc + PEGDMA + 1.0CNT ink is 7 times and the EPAc + PEGDMA + 2.0CNT ink is more than 21 times as viscous as the EPAc + PEGDMA ink.

The illustration in Figure 4c depicts that CNTs can change the transmission path of UV lights in the resin, which affects the curing of inks. In the curing process, UV light could reflect,

https://doi.org/10.1021/acsami.1c02624
ACS Appl. Mater. Interfaces 2021, 13, 18110−18119

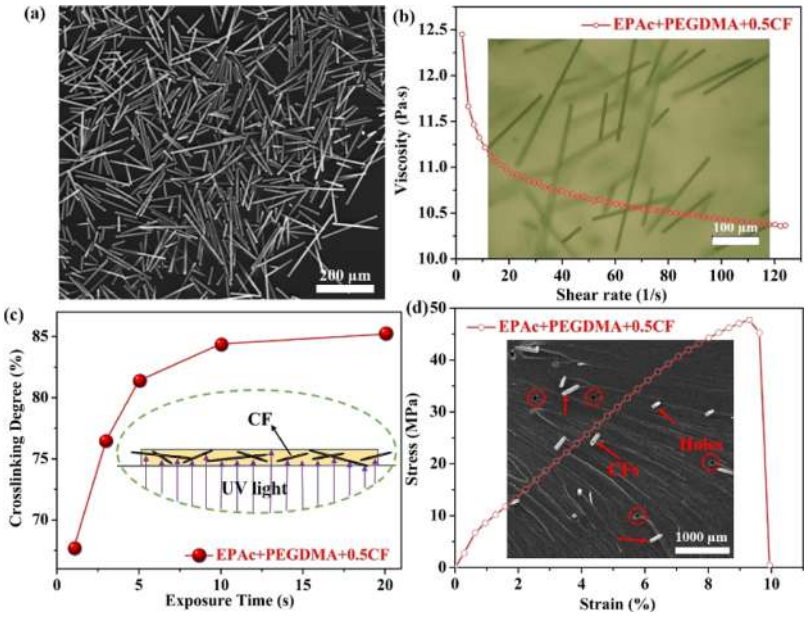

Figure 5. (a) SEM image of the additive 0.1−0.3 mm CFs; (b) viscosity curve of the EPAc + PEGDMA + 0.5CF ink and the inset: an optical microscope picture of CFs in the EPAc + PEGDMA resin; (c) cross-linking degree of the resin and the inset: schematic diagram of UV light path; and (d) stress−strain curve of the resin and the inset: a fracture surface SEM image of a tensile specimen.

interfere, diffract, and transmit, resulting in the loss of light energy. The inks containing CNTs are cured at different exposure times of 1, 3, 5, 10, and 20 s. The corresponding cross-linking degree is plotted as shown in Figure 4d. When the exposure time is less than 5 s, the cross-linking degree increases rapidly. When the exposure time is more than 5 s, its increase slumps. In addition, the absorption of CNT to UV light leads to a longer curing time of the composite ink. The optical micrographs of CNTs dispersed in the resin matrix and the printed pawl parts with different CNT contents are shown in Figure S5. The post-curing time of the three parts is 300 s. Two differences can be clearly seen in the side view of the three printed parts (see Figure 4e). One difference is that the surface roughness increases with the increase in CNT content. Another difference is that the thickness of the part printed with the EPAc + PEGDMA + 2.0CNT ink is significantly thinner than that printed with EPAc + PEGDMA + 0.5CNT and EPAc + PEGDMA + 1.0CNT inks at the same pre-job setting. The designed thickness of the three printed parts is 6.0 mm in the model. The actual thickness of the part printed with EPAc + PEGDMA + 2.0CNT is about 3.7 mm. For composite inks, the slice expose time is 3 s which is not enough to make a layer cured as design due to the high content (1.0 and 2.0 wt %) of CNTs, resulting in decreased thickness. The mechanical tensile test of the printed tensile specimen (see Figure 4f) shows that the addition of CNTs can enhance the tensile stress but significantly reduce the tensile strain compared with the result of EPAc + PEGDMA. The illustration shows the uneven fracture surface of the specimen, which is caused by the addition of CNTs.

In addition to CNTs, we also studied the effect of short CFs on the resin. The fibers were dipped in acetone for 24 h to remove surface coating and then rinsed with water three times before being put in the drying oven at 80 °C. The treated fibers were added into the EPAc + PEGDMA ink, stirred, and ultrasonically treated for 2 h. Figure 5a shows the SEM image of short CFs with a length of about 0.1−0.3 mm which is greater than the thickness of the printing layer (50 μm). Compared with the EPAc + PEGDMA + 0.5CNT ink, the initial viscosity of the EPAc + PEGDMA + 0.5CF ink is lower, which may be attributed to the nano-size effect of CNTs. The inset in Figure 5b is an optical micrograph of CFs dispersed in the EPAc + PEGDMA resin matrix. As demonstrated in Figure 5c, UV light penetrates more easily through the EPAc + PEGDMA + 0.5CF ink layer than the EPAc + PEGDMA + 0.5CNT ink layer. Therefore, when they are exposed to UV light for the same time, the cross-linking degree of EPAc + PEGDMA + 0.5CF is apparently higher than that of EPAc + PEGDMA + 0.5CNT, and the data are listed in Table S1. The EPAc + PEGDMA + 0.5CF specimen is post-cured for 180 s before a tensile test. In Figure 5d, the stress−strain curve of the printed specimen shows 10.6 MPa stress increase and 5.0% strain decrease compared to the result of EPAc + PEGDMA. The increase in stress is attributed to the CFs in the resin matrix. One end of the fibers and some holes can be clearly seen from the cross-section diagram in the illustration. The fibers are arranged in a two-dimensional orientation in a layer due to the extrusion of the printing platform during the printing process, which makes the composite anisotropic in mechanical properties.

The DMA results of EPAc + PEGDMA + 0.5CNT resin and EPAc + PEGDMA + 0.5CF resin are shown in Figure S6 and Table S2. T_g of EPAc + PEGDMA + 0.5CNT and EPAc + PEGDMA + 0.5CF is about 14.0 °C lower than that of EPAc + PEGDMA. The rubber elastic modulus of EPAc + PEGDMA + 0.5CF is 3.6 times that of EPAc + PEGDMA + 0.5CNT showing that the cross-linking density of EPAc + PEGDMA + 0.5CF is higher than that of EPAc + PEGDMA + 0.5CNT. As shown in Figure S7, the tensile specimens are printed and tested in the following two ways, named Mode A and Mode B. The printed samples based on EPAc + PEGDMA + 0.5CNT and EPAc + PEGDMA + 0.5CF in Mode B are tested and the results are exhibited in Table S3. The tensile force F applied to the tensile specimen printed in Mode A is parallel to the

https://doi.org/10.1021/acsami.1c02624
ACS Appl. Mater. Interfaces 2021, 13, 18110−18119

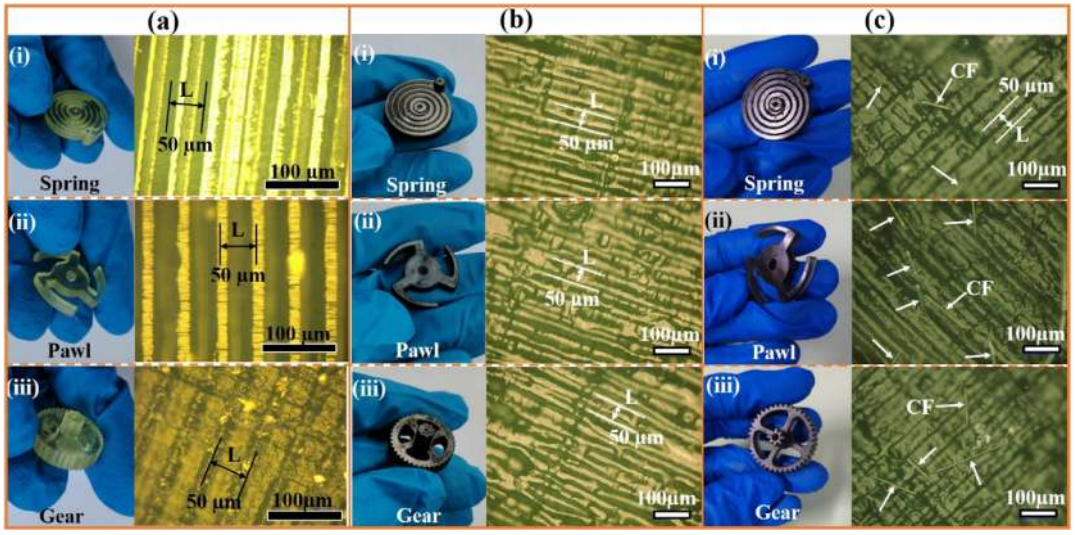

Figure 6. Printed parts [spiral spring (i), pawl (ii), and gear (iii)] and surface images of printed parts based on EPAc + PEGDMA resin (a), EPAc + PEGDMA + 0.5CNT resin (b), and EPAc + PEGDMA + 0.5CF resin (c).

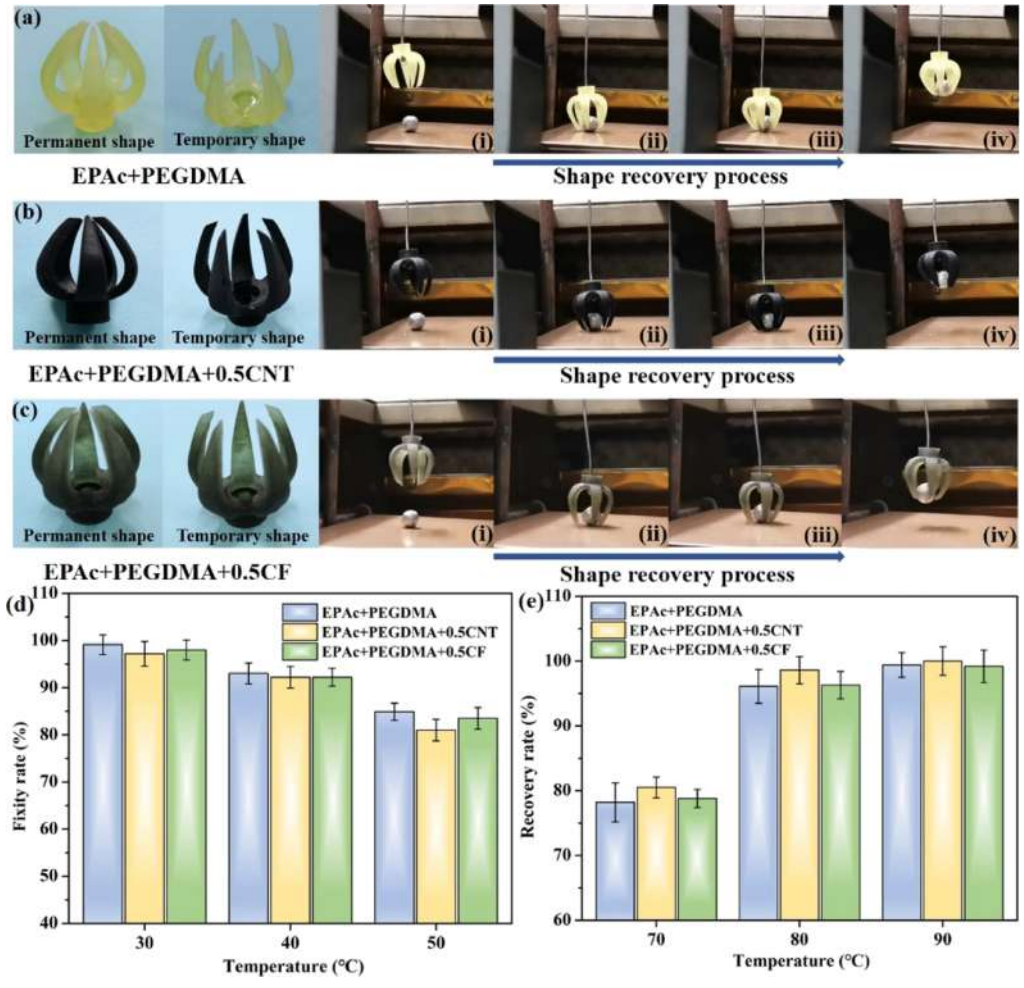

Figure 7. Shape recovery process of printed capture devices based on EPAc + PEGDMA resin (a), EPAc + PEGDMA + 0.5CNT resin (b), and EPAc + PEGDMA + 0.5CF resin (c); fixity rate (d); and recovery rate (e) of the three resins at different temperatures.

printing layers, and the tensile force applied to the tensile specimen printed in Mode B is perpendicular to the printing layers during the tensile process. For EPAc + PEGDMA + 0.5CNT, CNTs are randomly distributed in the resin, whose effect is the same in both modes. The tensile strength in Mode B is 11.7 MPa lower than that in Mode A. The decrease in tensile strength is mainly caused by interlaminar adhesion. For EPAc + PEGDMA + 0.5CF, the tensile strength in Mode B is

https://doi.org/10.1021/acsami.1c02624
ACS Appl. Mater. Interfaces 2021, 13, 18110−18119

3.9 MPa lower than that in Mode A. The decrease is mainly caused by the weak reinforcing effect of CFs between the layers and interlayer adhesion.

The addition of CNTs or CFs not only affects the tensile strength of composites, but also affects the printing process. The surface images of the parts printed with the EPAc + PEGDMA ink, EPAc + PEGDMA + 0.5CNT ink, and EPAc + PEGDMA + 0.5CF ink are exhibited in Figure 6 and their dimensions are shown in Figure S8. Optical microscopy of parts is performed using an optical microscope and the thickness of each slice is 50 μm. For EPAc + PEGDMA, the stripes as printing layers can be seen clearly. For EPAc + PEGDMA + 0.5CNT and EPAc + PEGDMA + 0.5CF, stripes are not as clear as EPAc + PEGDMA. Some humps as shown in Figure 6b may be caused by CNTs. CFs on the micron scale are easily observed in Figure 6c and are marked by white arrows.

The incorporation of carbon material can improve the thermal conductivity of the resin and accelerate the shape recovery process. To prove the improvement, three kinds of printed claw-like parts based on EPAc + PEGDMA, EPAc + PEGDMA + 0.5CNT, and EPAc + PEGDMA + 0.5CF are tested under the same conditions, whose permanent and temporary shapes are shown in Figures S9 and 7. Then, their grasping processes are studied and the whole process of the EPAc + PEGDMA claw grasping a tinfoil ball is within 170 s (Video 1), that of EPAc + PEGDMA + 0.5CNT claw is within 100 s (Video 2), and that of EPAc + PEGDMA + 0.5CF claw is within 120 s (Video 3). The demonstration shows that the thermal conductivity of the resin with CNTs is higher than that of the resin with CFs. Some printed samples (80 × 5 × 1 mm) are shaped into letter "U" to test R_f and R_r. The data of shape fixity rate and shape recovery rate at different temperatures are listed in Table S4. The results in Figure 7d show that R_f decreases as the measurement temperature increases. R_f is above 97.0% at 30 °C. R_f of EPAc + PEGDMA resin is the highest and that of EPAc + PEGDMA + 0.5CNT is the lowest, indicating that the addition of CNTs and CFs is not conducive to R_f. Figure 7e shows that the resins have higher R_r when the temperature is close to T_g. R_r is above 99.2% at 90 °C. In brief, EPAc + PEGDMA + 0.5CNT presents a shorter shape recovery time, higher R_r, and lower R_f under the same test conditions compared to EPAc + PEGDMA + 0.5CF, which is attributed to the excellent thermal conductivity of CNTs.

4. CONCLUSIONS

In summary, we develop a new type of black ink containing photosensitive epoxy, PEGDMA, and carbon fillers, which can be used for high-speed printing. Under UV irradiation, the ink can be quickly cured into high-performance resin, showing excellent thermodynamic properties and shape-memory effect. In addition, the curing conditions of CNT- and CF-filled epoxy composites are investigated preliminarily. Both CNTs and CFs can affect the way of light transmission, leading to the decrease in curing rate and cross-linking degree, which provides guidance for the exposure time of each layer during the printing process. CFs are superior to CNTs in improving the tensile strength, but CNTs play a greater role in the shape recovery process. It provides a new way for the efficient printing of shape memory thermosets to meet the requirements of deformable grabbing structures in space.

ASSOCIATED CONTENT

Supporting Information

The Supporting Information is available free of charge at https://pubs.acs.org/doi/10.1021/acsami.1c02624.

Addition esterification; ^{1}H NMR of EP and EPAc; FTIR spectra of EPAc and EPAc + PEGDMA resins with different exposure times; TGA of EPAc and EPAc + PEGDMA; DMA of EPAc + PEGDMA, EPAc + PEGDMA + 0.5CNT, and EPAc + PEGDMA + 0.5CF; stress−strain behaviors of anisotropic EPAc + PEGDMA + 0.5CNT and EPAc + PEGDMA + 0.5CF; and printed pawls and claw-like parts (PDF)

Shape-recovery process of printed capture device based on EPAc + PEGDMA resin; shape-recovery process of printed capture device based on EPAc + PEGDMA + 0.5CNT resin; and shape-recovery process of printed capture device based on EPAc + PEGDMA + 0.5CF resin (ZIP)

AUTHOR INFORMATION

Corresponding Author

Jinsong Leng − *Centre for Composite Materials and Structures, Harbin Institute of Technology (HIT), Harbin 150080, People's Republic of China;* orcid.org/0000-0001-5098-9871; Email: lengjs@hit.edu.cn

Authors

Linlin Wang − *Centre for Composite Materials and Structures, Harbin Institute of Technology (HIT), Harbin 150080, People's Republic of China*

Fenghua Zhang − *Centre for Composite Materials and Structures, Harbin Institute of Technology (HIT), Harbin 150080, People's Republic of China*

Yanju Liu − *Department of Astronautical Science and Mechanics, Harbin Institute of Technology (HIT), Harbin 150001, People's Republic of China*

Shanyi Du − *Centre for Composite Materials and Structures, Harbin Institute of Technology (HIT), Harbin 150080, People's Republic of China*

Complete contact information is available at: https://pubs.acs.org/10.1021/acsami.1c02624

Notes

The authors declare no competing financial interest.

ACKNOWLEDGMENTS

This work is supported by the National Natural Science Foundation of China (grant nos. 11632005 and 11802075).

REFERENCES

(1) Jena, R. K.; Dev, K.; Yue, C. Y.; Asundi, A. Effect of residual stresses in injection molded cyclic olefin copolymer during microfabrication: hot embossing as well as thermal bonding. *RSC Adv.* **2012**, *2*, 5717−5728.

(2) Hashizume, M.; Kunitake, T. Preparations of self-supporting nanofilms of metal oxides by casting processes. *Soft Matter* **2006**, *2*, 135−140.

(3) Sankhala, K.; Wieland, D. C. F.; Koll, J.; Radjabian, M.; Abetz, C.; Abetz, V. Self-assembly of block copolymers during hollow fiber spinning: an in situ small-angle X-ray scattering study. *Nanoscale* **2019**, *11*, 7634−7647.

(4) Tian, M.; Gao, W.; Hu, J.; Xu, X.; Ning, N.; Yu, B.; Zhang, L. Multidirectional Triple-Shape-Memory Polymer by Tunable Cross-

linking and Crystallization. *ACS Appl. Mater. Interfaces* **2020**, *12*, 6426−6435.
(5) Hagaman, D. E.; Leist, S.; Zhou, J.; Ji, H.-F. Photoactivated Polymeric Bilayer Actuators Fabricated via 3D Printing. *ACS Appl. Mater. Interfaces* **2018**, *10*, 27308−27315.
(6) Zhang, Y.; Yin, X.-Y.; Zheng, M.; Moorlag, C.; Yang, J.; Wang, Z. L. 3D printing of thermo reversible polyurethanes with targeted shape memory and precise in situ self-healing properties. *J. Mater. Chem. A* **2019**, *7*, 6972−6984.
(7) Peng, K.; Zhao, Y.; Shahab, S.; Mirzaeifar, R. Ductile Shape-Memory Polymer Composite with Enhanced Shape Recovery Ability. *ACS Appl. Mater. Interfaces* **2020**, *12*, 58295−58300.
(8) Zhao, W.; Zhang, F.; Leng, J.; Liu, Y. Personalized 4D printing of bioinspired tracheal scaffold concept based on magnetic stimulated shape memory composites. *Compos. Sci. Technol.* **2019**, *184*, 107866.
(9) Zhu, P.; Yang, W.; Wang, R.; Gao, S.; Li, B.; Li, Q. 4D Printing of Complex Structures with a Fast Response Time to Magnetic Stimulus. *ACS Appl. Mater. Interfaces* **2018**, *10*, 36435−36442.
(10) Duigou, A. L.; Chabaud, G.; Scarpa, F.; Castro, M. Bioinspired Electro-Thermo-Hygro Reversible Shape-Changing Materials by 4D Printing. *Adv. Funct. Mater.* **2019**, *29*, 1903280.
(11) Cheng, C.-Y.; Xie, H.; Xu, Z.-y.; Li, L.; Jiang, M. N.; Tang, L.; Yang, K. K.; Wang, Y. Z. 4D printing of shape memory aliphatic copolyester via UV-assisted FDM strategy for medical protective devices. *Chem. Eng. J.* **2020**, *396*, 125242.
(12) Lin, C.; Lv, J.; Li, Y.; Zhang, F.; Li, J.; Liu, Y.; Liu, L.; Leng, J. 4D-Printed Biodegradable and Remotely Controllable Shape Memory Occlusion Devices. *Adv. Funct. Mater.* **2019**, *29*, 1906569.
(13) Zarek, M.; Layani, M.; Cooperstein, I.; Sachyani, E.; Cohn, D.; Magdassi, S. 3D Printing of Shape Memory Polymers for Flexible Electronic Devices. *Adv. Mater.* **2016**, *28*, 4449−4454.
(14) Zhang, W.; Wang, H.; Wang, H.; Chan, J. Y. E.; Liu, H.; Zhang, B.; Zhang, Y. F.; Agarwal, K.; Yang, X.; Ranganath, A. S.; Low, H. Y.; Ge, Q.; Yang, J. K. W. Structural multi-colour invisible inks with submicron 4D printing of shape memory polymers. *Nat. Commun.* **2021**, *12*, 112.
(15) Zhang, F.; Wang, L.; Zheng, Z.; Liu, Y.; Leng, J. Magnetic programming of 4D printed shape memory composite structures. *Composites, Part A* **2019**, *125*, 105571.
(16) Ryan, K. R.; Down, M. P.; Banks, C. E. Future of additive manufacturing: Overview of 4D and 3D printed smart and advanced materials and their applications. *Chem. Eng. J.* **2021**, *403*, 126162.
(17) Peng, B.; Yang, Y.; Gu, K.; Amis, E. J.; Cavicchi, K. A. Digital Light Processing 3D Printing of Triple Shape Memory Polymer for Sequential Shape Shifting. *ACS Mater. Lett.* **2019**, *1*, 410−417.
(18) Wang, Y.; Raman Pillai, S. K.; Che, J.; Chan-Park, M. B. High Interlaminar Shear Strength Enhancement of Carbon Fiber/Epoxy Composite through Fiber- and Matrix-Anchored Carbon Nanotube Networks. *ACS Appl. Mater. Interfaces* **2017**, *9*, 8960−8966.
(19) Matsuura, K.; Umahara, Y.; Gotoh, K.; Hoshijima, Y.; Ishida, H. Surface modification effects on the tensile properties of functionalised graphene oxide epoxy films. *RSC Adv.* **2018**, *8*, 9677−9684.
(20) Xu, W.; Chen, J.; Chen, S.; Chen, Q.; Lin, J.; Liu, H. Study on the Compatibilizing Effect of Janus Particles on Liquid Isoprene Rubber/Epoxy Resin Composite Materials. *Ind. Eng. Chem. Res.* **2017**, *56*, 14060−14068.
(21) Yang, G.; Cui, J.; Ohki, Y.; Wang, D.; Li, Y.; Tao, K. Dielectric and relaxation properties of composites of epoxy resin and hyperbranched-polyester-treated nanosilica. *RSC Adv.* **2018**, *8*, 30669−30677.
(22) Rodriguez, J. N.; Zhu, C.; Duoss, E. B.; Wilson, T. S.; Spadaccini, C. M.; Lewicki, J. P. Shape-morphing composites with designed micro-architectures. *Sci. Rep.* **2016**, *6*, 27933.
(23) Hao, W.; Liu, Y.; Zhou, H.; Chen, H.; Fang, D. Preparation and characterization of 3D printed continuous carbon fiber reinforced thermosetting composites. *Polym. Test.* **2018**, *65*, 29−34.
(24) Kuang, X.; Zhao, Z.; Chen, K.; Fang, D.; Kang, G.; Qi, H. J. High-Speed 3D Printing of High-Performance Thermosetting Polymers via Two-Stage Curing. *Macromol. Rapid Commun.* **2018**, *39*, 1700809.
(25) Chen, K.; Kuang, X.; Li, V.; Kang, G.; Qi, H. J. Fabrication of tough epoxy with shape memory effects by UV-assisted direct-ink write printing. *Soft Matter* **2018**, *14*, 1879−1886.
(26) Lu, C.; Wang, C.; Yu, J.; Wang, J.; Chu, F. Two-Step 3D-Printing Approach toward Sustainable, Repairable, Fluorescent Shape-Memory Thermosets Derived from Cellulose and Rosin. *ChemSusChem* **2020**, *13*, 893−902.
(27) Chiappone, A.; Roppolo, I.; Naretto, E.; Fantino, E.; Calignano, F.; Sangermano, M.; Pirri, F. Study of graphene oxide-based 3D printable composites: Effect of the in situ reduction. *Composites, Part B* **2017**, *124*, 9−15.
(28) Mantelli, A.; Romani, A.; Suriano, R.; Diani, M.; Colledani, M.; Sarlin, E.; Turri, S.; Levi, M. UV-Assisted 3D Printing of Polymer Composites from Thermally and Mechanically Recycled Carbon Fibers. *Polymers* **2021**, *13*, 726.
(29) Mantelli, A.; Levi, M.; Turri, S.; Suriano, R. Remanufacturing of end-of-life glass-fiber reinforced composites via UV-assisted 3D printing. *Rapid Prototyp. J.* **2019**, *26*, 981−992.
(30) Compton, B. G.; Hmeidat, N. S.; Pack, R. C.; Heres, M. F.; Sangoro, J. R. Electrical and Mechanical Properties of 3D-Printed Graphene-Reinforced Epoxy. *JOM* **2018**, *70*, 292−297.
(31) Trigg, E. B.; Hmeidat, N. S.; Smieska, L. M.; Woll, A. R.; Compton, B. G.; Koerner, H. Revealing filler morphology in 3D-printed thermoset nanocomposites by scanning microbeam X-ray scattering. *Addit. Manuf.* **2021**, *37*, 101729.
(32) Choong, Y. Y. C.; Maleksaeedi, S.; Eng, H.; Yu, S.; Wei, J.; Su, P.-C. High speed 4D printing of shape memory polymers with nanosilica. *Appl. Mater. Today* **2020**, *18*, 100515.
(33) Kuang, X.; Chen, K.; Dunn, C. K.; Wu, J.; Li, V. C. F.; Qi, H. J. 3D Printing of Highly Stretchable, Shape-Memory, and Self-Healing Elastomer toward Novel 4D Printing. *ACS Appl. Mater. Interfaces* **2018**, *10*, 7381−7388.
(34) Ren, L.; Li, B.; Song, Z.; Liu, Q.; Ren, L.; Zhou, X. Bioinspired fiber-regulated composite with tunable permanent shape and shape memory properties via 3d magnetic printing. *Composites, Part B* **2019**, *164*, 458−466.
(35) Ren, L.; Li, B.; Song, Z.; Liu, Q.; Ren, L.; Zhou, X. 3D printing of structural gradient soft actuators by variation of bioinspired architectures. *J. Mater. Sci.* **2019**, *54*, 6542−6551.
(36) Azukizawa, S.; Shinoda, H.; Tokumaru, K.; Tsumori, F. 3D Printing System of Magnetic Anisotropy for Artificial Cilia. *J. Photopolym. Sci. Technol.* **2018**, *31*, 139−144.
(37) Kim, T.; Trangkanukulkij, R.; Kim, W. S. Nozzle Shape Guided Filler Orientation in 3D Printed Photocurable Nanocomposites. *Sci. Rep.* **2018**, *8*, 3805.
(38) Feng, Y.; Hu, J.; Wang, F.; Huang, Q.; Peng, C.; Xu, Z. Synthesizing promising epoxy acrylate prepolymers applied in ultraviolet cured adhesives based on esterification reaction. *Mater. Res. Express* **2018**, *5*, 065321.
(39) Çanak, T. Ç.; Kaya, K.; Serhatlı, I. E. Boron containing UV-curable epoxy acrylate coatings. *Prog. Org. Coat.* **2014**, *77*, 1911−1918.
(40) Tang, E.; Bian, F.; Klein, A.; El-Aasser, M.; Liu, S.; Yuan, M.; Zhao, D. Fabrication of an epoxy graft poly(St-acrylate) composite latex and its functional properties as a steel coating. *Prog. Org. Coat.* **2014**, *77*, 1854−1860.
(41) Chen, J.; Zhou, Y. M.; Ding, Q. H.; He, M. An UV-curable epoxy acrylate oligomer with high refractive index containing fluorene: Preparation, characterization, and application. *J. Appl. Polym. Sci.* **2015**, *132*, 42386.
(42) Luo, C.; Zhang, B.; Zhang, W.; Yuan, C.; Dunn, M.; Ge, Q.; Yu, K. Chemomechanics of dual-stage reprocessable thermosets. *J. Mech. Phys. Solids* **2019**, *126*, 168−186.
(43) Bell, C. L.; Peppas, N. A. Equilibrium and Dynamic Swelling of Polyacrylates. *Polym. Eng. Sci.* **1996**, *36*, 1856−1861.

https://doi.org/10.1021/acsami.1c02624
ACS Appl. Mater. Interfaces 2021, 13, 18110−18119

(44) Wu, H.; Chen, P.; Yan, C.; Cai, C.; Shi, Y. Four-dimensional printing of a novel acrylate-based shape memory polymer using digital light processing. *Mater. Des.* **2019**, *171*, 107704.
(45) Miao, S.; Zhu, W.; Castro, N. J.; Nowicki, M.; Zhou, X.; Cui, H.; Fisher, J. P.; Zhang, L. G. 4D printing smart biomedical scaffolds with novel soybean oil epoxidized acrylate. *Sci. Rep.* **2016**, *6*, 27226.
(46) Wu, Q.; Hu, Y.; Tang, J.; Zhang, J.; Wang, C.; Shang, Q.; Feng, G.; Liu, C.; Zhou, Y.; Lei, W. High-Performance Soybean-Oil-Based Epoxy Acrylate Resins: "Green" Synthesis and Application in UV-Curable Coatings. *ACS Sustainable Chem. Eng.* **2018**, *6*, 8340−8349.
(47) Yu, R.; Yang, X.; Zhang, Y.; Zhao, X.; Wu, X.; Zhao, T.; Zhao, Y.; Huang, W. Three-Dimensional Printing of Shape Memory Composites with Epoxy-Acrylate Hybrid Photopolymer. *ACS Appl. Mater. Interfaces* **2017**, *9*, 1820−1829.

https://doi.org/10.1021/acsami.1c02624
ACS Appl. Mater. Interfaces 2021, 13, 18110−18119